

Surface superconducting states and paramagnetism in mesoscopic superconductors

C. Meyers*

Condensed Matter Theory Group, CPMOH
CNRS UMR-5798, Université Bordeaux 1,
33405 Talence Cedex, France

PACS numbers: 73.25+i 74.25Ha 74.78Na 75.20-g

Abstract

In the framework of the Ginzburg-Landau equation, the temperature dependence of the upper critical field of small ring-like superconductors is studied. At equilibrium small parts of the phase diagram show paramagnetism for width / radius ratios below 0.85. Their number and extension increase with the size of the hole. In these regions, only the inner part of the ring shows a positive magnetic moment. The order parameter density profile appears to change, when crossing a first order transition line, which separates different angular momentum values, and we clarify the relationship between the localization of superconductivity nucleation and paramagnetism of those samples.

1 Introduction

The paramagnetic Meissner effect (PME) observed in small superconducting samples simply expresses the fact that the energy of those samples decreases upon an increasing magnetic field. A reentrant (H,T) phase diagram is one

*email: meyers@cpmoh.u-bordeaux.fr

of the signals that characterizes this effect. This surprising effect has been seen both in conventional [1][2] and in high Tc superconductors [3].

The behavior of nanometer-scale superconducting grains [4], which shows Pauli paramagnetism [5] in addition to other striking properties of finite electron systems, is outside the scope of this work which relies on the Ginzburg-Landau equation.

Metastability is one of the major ingredients that have been put forward to explain PME in conventional superconductors [6]. For example, in the Ginzburg-Landau approach of small size cylindrical samples at the upper critical field, the disbalance of the screening currents leads to a positive magnetic moment [7]. But, in this case if the equilibrium transitions are only allowed, the PME disappears [7], and many mechanisms causing non equilibrium flux configuration have been proposed [6].

However PME is known to occur for minimal energy configurations of some mesoscopic objects: the Little-Parks [8] ring is the most simple example that shows an alternating sequence of diamagnetic and paramagnetic responses as the magnetic field is increased. On the theoretical side this general behavior is known to be shared by all loop-like samples and moreover that PME appears to be stable against thermic fluctuations [9].

In the framework of the London approximation of the vortex phase of small superconducting disks, we have obtained magnetization curves which showed a PME, in good agreement with the experimental observation [2], and made the analogy with the Little-Parks ring to interpret such a behavior of stable configurations [10].

The aim of this paper is to give the reader a simple example of a mesoscopic ring-like superconducting film of which the paramagnetic response of the stable configurations can be tuned with the size of the central hole, and to show at which part of the ring (inner or outer) the nucleation of superconductivity is localized.

In Section 2 the upper critical field H_{c3}^* is calculated in the framework of the Ginzburg-Landau equation, and, if the size of the hole is large enough, the parts of the phase diagram where PME takes place are found. In Section 3 we show the two regions of the ring with opposite supercurrents which might give rise to a global positive magnetic moment. In Section 4 we give in more details our results for a ring with a small hole with $width / Radius = 0.75$ for which there is only one paramagnetic domain and we also show the order parameter density profile that changes drastically when crossing the first order line. Our conclusions are drawn in the last section.

2 Nucleation of superconductivity near the edges of a ring

We shall follow quite closely the method of Bezryadin, Buzdin and Pannetier [11] in the case of a circular hole or of a disk[12], in order to obtain the phase diagram of a circular ring of external radius R and width d under a uniform magnetic field H normal to the plane of the film sample.

In the case of a thin film of thickness ϵ the effective screening length, $\lambda_{eff} = \lambda^2/\epsilon$, becomes very large and we may neglect the magnetic field energy in the Ginzburg-Landau (GL) free energy functional:

$$F = \int \left(a |\Psi|^2 + \frac{b}{2} |\Psi|^4 + \frac{1}{4m} \left| \left(-i\hbar \vec{\nabla} - \frac{2e}{c} \vec{\mathbf{A}} \right) \Psi \right|^2 \right) dV$$

where $a = \alpha(T - T_0)$.

Moreover due to the small size of the sample, we can take for the vector potential $\vec{\mathbf{A}}$ the potential of the uniform external applied field H :

$$\vec{\mathbf{A}} = \frac{1}{2}(\vec{\mathbf{H}} \times \vec{\mathbf{r}})$$

Using polar coordinates (ρ, φ) , the equation for the normalized order parameter ψ is:

$$\frac{d^2}{dx^2} \psi + \frac{1}{x} \frac{d}{dx} \psi - \left[\frac{i}{x} \frac{\partial}{\partial \varphi} + \frac{\phi}{\phi_0} x \right]^2 \psi + \frac{R^2}{\xi^2} (\psi - \psi^3) = 0$$

where $x = \rho/R$, $\psi = \Psi / \sqrt{|a|/b}$, $\xi^2 = \hbar^2 / 4m |a|$, $\phi_0 = \pi \hbar c / e$, and $\phi = \pi R^2 H$ is the flux of the magnetic field across the plain disk (with no hole).

In order to obtain the upper critical field H_{c3}^* [13], using the linearized version of the GL equation, we search for solutions of definite angular momentum n of the form:

$$\psi_n(x, \varphi) = f_n(x) \exp(in\varphi).$$

Then, in the present gauge, the super-current is tangent to the two circular insulating boundaries of the ring, and we may take the boundary conditions of the GL equation as follows:

$$\frac{d}{dx}f|_{x=1} = 0 \text{ , and } \frac{d}{dx}f|_{x=1-d/R} = 0 \text{ .}$$

After reduction to Kummer's equation, the general solution can be expressed as the linear combination of two confluent hypergeometric functions M and U [14] as follows:

$$f_n(x) = x^n \exp\left(-\frac{x^2}{2} \frac{\phi}{\phi_0}\right) \left\{ A M\left(Y, n+1, x^2 \frac{\phi}{\phi_0}\right) + B U\left(Y, n+1, x^2 \frac{\phi}{\phi_0}\right) \right\}$$

where $Y = \frac{1}{2} - \frac{1}{4} \frac{R^2}{\xi^2} \frac{\phi_0}{\phi}$, and where the two constants A and B have to be determined using the boundary conditions.

In practice, we have first obtained the ratio A/B in terms of ϕ , R^2/ξ^2 and n using the first condition, while the second condition has been numerically solved and allows us to obtain R^2/ξ^2 versus ϕ for each n . Then, for a given flux ϕ , the critical line $T_c(\phi)$ is obtained by choosing the angular momentum value which minimizes R^2/ξ^2 [11]. The limiting cases of either a plain disk or a circular hole can be reached, using the same procedure, with $B = 0$ in the first case and with $A = 0$ in the second one. The Little-Parks ring [8] , can be recovered using a very small value of d/R , as shown on figure 1 . We see that paramagnetism starts just after the transition between angular momentum states $J-1 \rightarrow J$ and disappears for $\phi/\phi_0 \geq J$, until the next transition occurs. On figure 2 we give the H_{c3}^* line for a ring with $d/R = 0.5$. The cusps, associated to jumps of the angular momentum, are clearly seen and three small paramagnetic domains are located above these transitions. For sake of comparison the full disk H_{c3}^* curve is shown on figure 3 , on which no such domains are seen; such oscillations have been observed on micron-sized superconducting disks[12]. Our results give $d/R \approx 0.85$ as the value under which paramagnetic domains are observed.

3 Magnetic moment and supercurrents

In the state f_n of angular momentum n , the magnetic moment $M = -\partial F / \partial H$ can be written as:

$$M = \frac{\phi_0}{(2\pi\lambda)^2} \pi R^2 \epsilon_{film} \int_{1-d/R}^1 f_n(x)^2 \left(n - \frac{\phi}{\phi_0} x^2\right) x dx.$$

In fact the local density of magnetic moment is related to the value of the supercurrent:

$$\mathbf{J} = \frac{\hbar}{4m} (\Psi^* \nabla \Psi - \Psi \nabla \Psi^*) - \frac{e}{2mc} \mathbf{A} |\Psi|^2$$

of which the components are:

$$J_\varphi = \frac{f_n(x)^2}{x} \left(n - \frac{\phi}{\phi_0} x^2\right) \quad \text{and} \quad J_\rho = 0$$

For a given flux and angular momentum, and when the ring is crossed from the inner edge ($x = 1 - d/R$) up to the outer one ($x = 1$), three various situations can be encountered according to the sign of J_φ :

- The radial supercurrent density is negative everywhere on the ring for $\frac{\phi}{\phi_0} > \frac{n}{(1-d/R)^2}$. This gives a uniform standard diamagnetic response.
- The radial supercurrent density is positive everywhere on the ring for $\frac{\phi}{\phi_0} < n$ and gives a uniform paramagnetic response
- The current flows changes its sign at a point $x_0 = \sqrt{\frac{\phi_0}{\phi} n}$. Thus one can distinguish two different regions on the ring: the inner part which contributes positively to the total magnetic moment and the outer part which gives a diamagnetic contribution, with currents in the two regions flowing in opposite directions.

Let us comment Figures 1-3 on this point. The ideal Little-Parks ring of Fig1 (with $d/R \approx 0$) shows a sequence of uniform responses: $J = 0$ is

diamagnetic, whereas the reentrant part of $J = 1$ is paramagnetic, etc... and the supercurrent changes its sign for all half-integer values of $\frac{\phi}{\phi_0}$. Fig2, which depicts the behavior of a thicker ring (with $d/R = 0.5$), shows that apart the standard uniform diamagnetic response of the $J = 0$ state, the $J = 1$ state gives a uniform paramagnetic response for small fields $\frac{\phi}{\phi_0} < 1$. The magnetization of all the other states results of the competition between the inner and the outer currents. The case of the plain disk (Fig3) is interesting although no paramagnetism is observed on the global magnetization: all the non-zero angular momentum states have a central paramagnetic response and a larger diamagnetic one located on the periphery of the disk.

4 Paramagnetism in a disk with a small hole

In this section, we have choosen to treat more extensively the particular case of a small hole, $d/R = 0.75$, by solving the non-linear Ginzburg-Landau equation. This allows us to enter the superconducting region, and compute the densities of both the order parameter and the magnetization. In fact it can be shown that mixture of different angular momentum states can be neglected if only the lowest energy is searched for, so that we shall not consider such mixtures.

Because the two boundary conditions restrict ψ at two different points, namely $x = 1 - d/R$ and $x = 1$, we have solved the non-linear GL equation in two steps. We have used standard numerical routines which allowed us to obtain $f_n(x)$ given the initial values $f_n(1)$ and $df_n/dx|_{x=1} = 0$, then $f_n(1)$ is found by solving $df_n/dx|_{x=1-d/R} = 0$ for $f_n(1)$.

The H_{c3}^* line for the ring with $d/R = 0.75$ is drawn on Fig. 4. Only one small paramagnetic domain shows up for fluxes $1.4 \lesssim \phi/\phi_0 \lesssim 1.8$ with $J = 1$. On the inset of Fig 4, which is a zoom of the paramagnetic region, we have drawn a fixed temperature path (A-B) with $R^2/\xi^2 = 1.2$ which crosses the first order transition line separating the $J = 0$ and $J = 1$ phases. A fixed flux path (C-B) with $\phi/\phi_0 = 1.625$ which lies entirely in the paramagnetic phase is also shown. The field dependence of the magnetization versus flux along the path (A-B) is given on Fig 5a, on which one sees the jump of the magnetic moment to a positive value when the first order line is crossed. This behavior should be compared with the smooth one of the magnetization along

path (C-B), in the paramagnetic phase at fixed field and versus temperature, on Fig 5b.

We now give on Fig 6 the magnetization density at points A and B versus ρ/R , i.e. when the ring is crossed from the inner circle to the outer one. As already explained in the previous section, one clearly sees that the inner part is paramagnetic while the outer one is diamagnetic and that the balance of the two results in a small PME effect. Let us stress that, following this line of argument, and as said for disks in the previous section, one should observe for disks with very small holes a small domain with a positive local magnetic moment (around the hole) while there is no global PME effect.

We discuss now the order parameter distribution across the ring. On Fig 7, comparing these densities, we find that the order parameter is larger in the inner part than in the outer part, at point A i.e. in the diamagnetic region. On the contrary, in the paramagnetic region, at points B, the order parameter is 30% larger in the vicinity of the outer edge than around the hole.

Figure 8 shows how the order parameter density profile changes when crossing the first order transition at $\phi/\phi_0 = 1.4$ at fixed temperature $R^2/\xi^2 = 1.2$. We have plotted the values of $|\psi_J|$ on the two, inner and outer, boundaries of the ring for $J = 0$ before the transition and for $J = 1$ after.

It is worthwhile to notice that the regions of the ring where the order parameter is the largest, changes as the first order line is crossed, passing from the inner part before the transition to the outer one after. We have checked on the example of $d/R = 0.5$ that this result should be general. In this last case it is observed that, sweeping the temperature range of $J = 1$ from one transition point ($J = 0 \rightarrow J = 1$) to the next one ($J = 1 \rightarrow J = 2$), the order parameter profile $|\psi_1|$ evolves from more populated on the inner edge to more populated on the outer one. Let us note that, even though the superconducting parameter is maximal in this last region, a paramagnetic effect arises because of the large inner part of the disk in which the magnetization density is positive (see Fig. 6).

5 Conclusions

The paramagnetism of a mesoscopic object can obviously be due to any mechanism leading to non equilibrium configurations. However, at equilibrium,

the PME depends strongly on the geometry of the sample and presumably can be observed in many cases much more involved than the toy model presented here. Here we have shown that the giant vortex state of a pierced disk can exhibit PME in minimal energy configurations. The size of the hole controls both the number and extension of the paramagnetic domains. Increase of the field at fixed temperature to enter those domains causes the order parameter to jump from inner to outer localization. The present approach does not explain the PME seen on the surface superconducting states of 1:4 elongated ellipses [15] for which the PME in an asymmetric ring should be studied. Paramagnetic Meissner effect in a multiply-connected array of Josephson junctions has been reported [16] for which the diamagnetic current flows on the exterior plaquettes whereas the paramagnetic current flows in the inside of the sample; this is very similar to that we have described here.

6 Acknowledgements

A. Buzdin is warmly thanked for his interest in this work and for numerous and helpful discussions.

References

- [1] D.J. Thompson, M.S.M. Minhaj, L.E. Wenger and J.T. Chen, Phys. Lett. **75**, 529 (1995);
P. Kostic, A.P. Paulikas, U. Welp, V.R. Todt, C. Gu, U. Geiser, J.M. Williams, K.D. Carlson and R.A. Klemm, Phys. Rev. **B 53**, 791 (1996);
A. Terentiev, D.B. Watkins and L.E.D. Long, Phys. Rev. **B 60**, R761 (1999).
- [2] A. S. Geim, S. V. Dubonos, J. G. S. Lok, M. Henini and J. C. Mann, Nature (London) **396**, 144 (1998).
- [3] W. Braunisch, N. Knauf, V. Kataev, A. Grutz, A. Kock, B. Roden, D. Khomskii and D. Wohlleben, Phys. Rev. Lett. **68**, 1908 (1992) and W. Braunisch, N. Knauf, B. Bauer, A. Kock, A. Becker, B. Freitag, A. Grutz, V. Kataev, S. Neuhausen, B. Roden, D. Khomskii and D. Wohlleben, Phys. Rev. **B 48**, 4030 (1993);
B. Schliepe, M. Stindtmann, I. Nikolic, and K. Baberschke, Phys. Rev.

- B 47**, 8331 (1993);
 S. Riedling, G. Brauchle, R. Lucht, K. Rohberg, and H. V. Lohneysen,
 Phys. Rev. **B 49**, 13283 (1994);
 U. Onbasli, Y.T. Wang, A. Naziripour, R. Tello, W. Kielh, and A. M.
 Hermann, Phys. Stat. Sol. **B 194**, 371 (1996);
 G.S. Okram, D.T. Adroja, B.D. Paladia, O. Prakash, and P.A.J. de
 Groot, J. Phys.: Cond. Mat. **9**, L525 (1997).
- [4] J. von Delft and D.C. Ralph, Phys. Rep. **345** (2001) 61 ;
 N. Canossa and R. Rossignoli, Physica **B 320** (2002) 319.
- [5] A.M. Clogston, Phys. Rev. Lett. **9** (1962) 266 ;
 B.S. Chandrasekhar, Appl. Phys. Lett. **1** (1962) 7;
 K. Maki and T. Tsuneto, Prog. Theor. Phys. **31** (1964) 945.
- [6] A. E. Koshelev and A. I. Larkin, Phys. Rev. **B 52** (1995) 13559.
 V. V. Moschalkov, X. G. Qiu and V. Bruyndoncx, Phys. Rev. **B 55**
 (1999) 11793.
 P. S. Deo, V. A. Schweigert, F. M. Peeters, and A. K. Geim, Phys. Rev.
 Lett. **79** (1997) 4653.
 P. S. Deo, V. A. Schweigert and F. M. Peeters, Phys. Rev. **B 59** (1999)
 6039.
- [7] G. F. Zarkov, Phys. Rev. **B 63** (2001) 214502.
- [8] W. A. Little and R. D. Parks, Phys. Rev. Lett. **9** (1962) 9; Phys. Rev.
A 133 (1964) 97.
- [9] M. Daumens, C. Meyers and A. Buzdin, Phys. Lett. **A 248** (1998) 445.
- [10] C. Meyers and M. Daumens, Phys. Rev. **B 62** (2000) 9762.
- [11] A. Bezryadin, A. Buzdin and B. Pannetier, Phys. Rev. **B 51** (1995) 3718.
- [12] O. Buisson, P. Gandit, R. Rammal, Y. Y. Wang and B. Pannetier,
 Phys. Lett. **A 150** (1990) 36.
- [13] D. Saint James and P. G. de Gennes, Phys. Lett. **7** (1963) 306.
- [14] Handbok of Mathematical Functions, edited by M. Abramowitz and I.
 A. Stegun (Dover, New York, 1970), p 504.

- [15] C. Meyers, M. Daumens and A. Buzdin, *Physica C* **325** (1999) 118 [See Fig 7 for $b/a = 0.25$].
- [16] A.P. Nielsen, A. B. Cawthorne, P. Barbara, F. C. Wellstood, C. J. Lobb, R. S. Newrock and M. G. Forrester, *Phys. Rev. B* **62** (2000) 1438 .
- [17] P. G. De Gennes, *Superconductivity of Metals and Alloys* (Benjamin, New York,1996).
- [18] A. A. Abrikosov, *Fundamentals of Theory of Metals*, (North-Holland, Amsterdam, 1988).

Figure captions

Figure 1. The phase diagram of a very thin ring with $d/R = 0.01$, versus normalized temperature $R^2 / \xi^2 \sim 1 - T / T_c$ and flux ϕ / ϕ_0 in flux quantum units. The surface superconducting critical line Hc_3 has been drawn for the first three angular momentum values.

Figure 2. The upper critical field Hc_3 for a ring with $d/R = 0.5$. The first order lines which separate domains of different angular momentum are drawn as thin full vertical lines, whereas vertical dashed lines mark the expected boundary of each paramagnetic region. The present study is valid to the right hand side of the Hc_2 line which has been shown for comparison (for the bulk material) .

Figure 3. The upper critical field Hc_3 for full disk with $d/R = 1$.

Figure 4. The phase diagram of a disk with a small hole $d/R = 0.75$, in the vicinity of the upper critical field Hc_3 . The inset plot shows a zoom of the region $1.2 \lesssim \phi/\phi_0 \lesssim 1.8$ in which a paramagnetic effect is expected.

Figure 5a. The magnetization at fixed normalized temperature $R^2 / \xi^2 = 1.2$ versus flux along the path A-B (See the inset graph of Fig. 4). The magnetization jumps to small positive values after the transition.

Figure 5b. The magnetization in the paramagnetic region at fixed flux $\phi/\phi_0 \lesssim 1.6$ versus temperature, along the path C-B (See the inset graph of Fig. 4).

Figure 6. The magnetization distribution across the ring, at point A (full line) and at point B (dashed line) (for A and B see the inset graph of Fig. 4).

Figure 7. Order parameter density at point A, before the transition , and at point B, in the paramagnetic region, versus the radial variable $1 - d/R < \rho/R < 1$.

Figure 8. The order parameter density profile oscillation when crossing the first order transition at $\phi/\phi_0 = 1.4$ for a ring with $d/R = 0.75$. The inner edge is more superconducting than the outer one before the transition, whereas the reverse situation occurs in the paramagnetic phase.

Fig 1

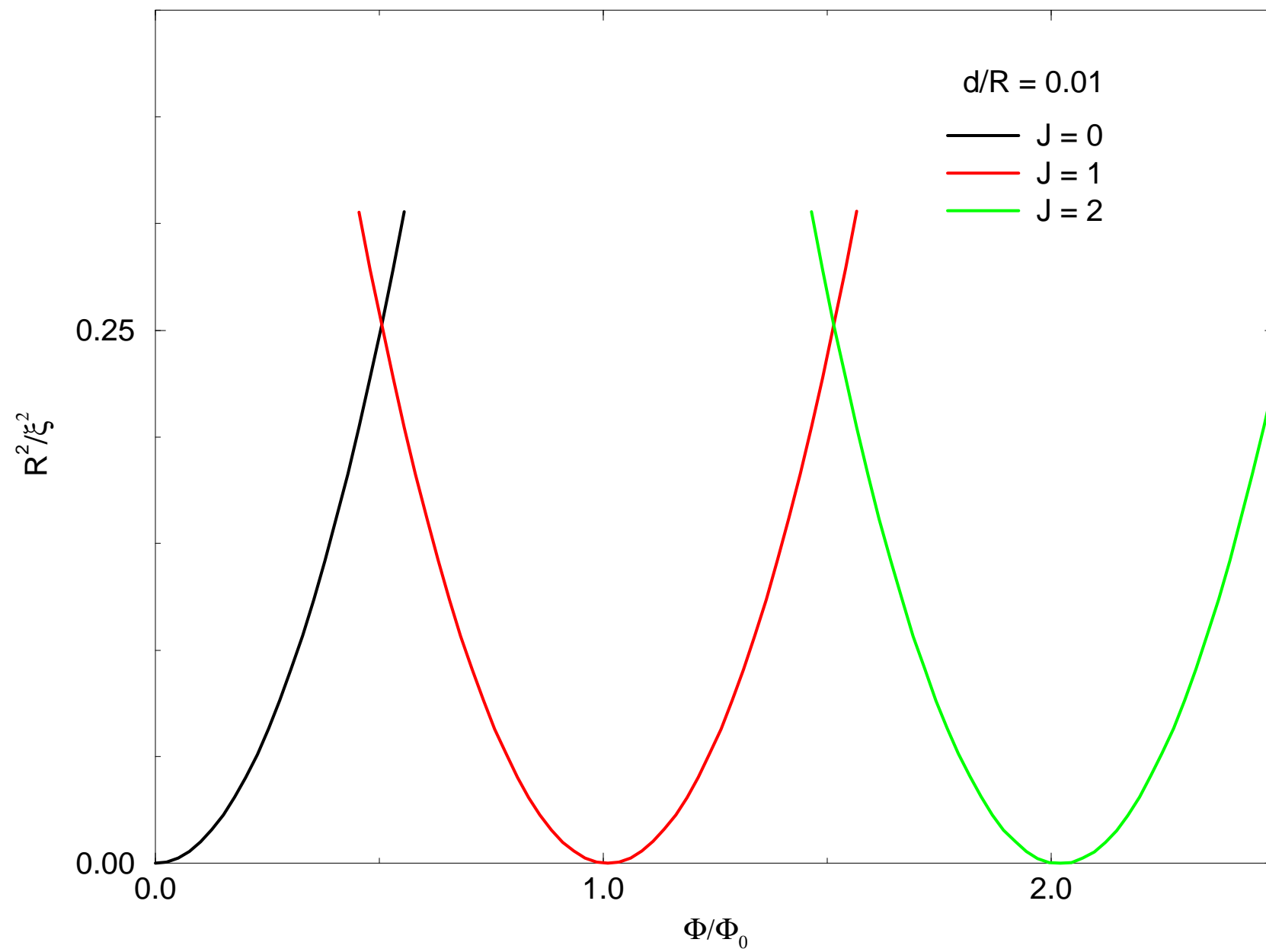


Fig 2

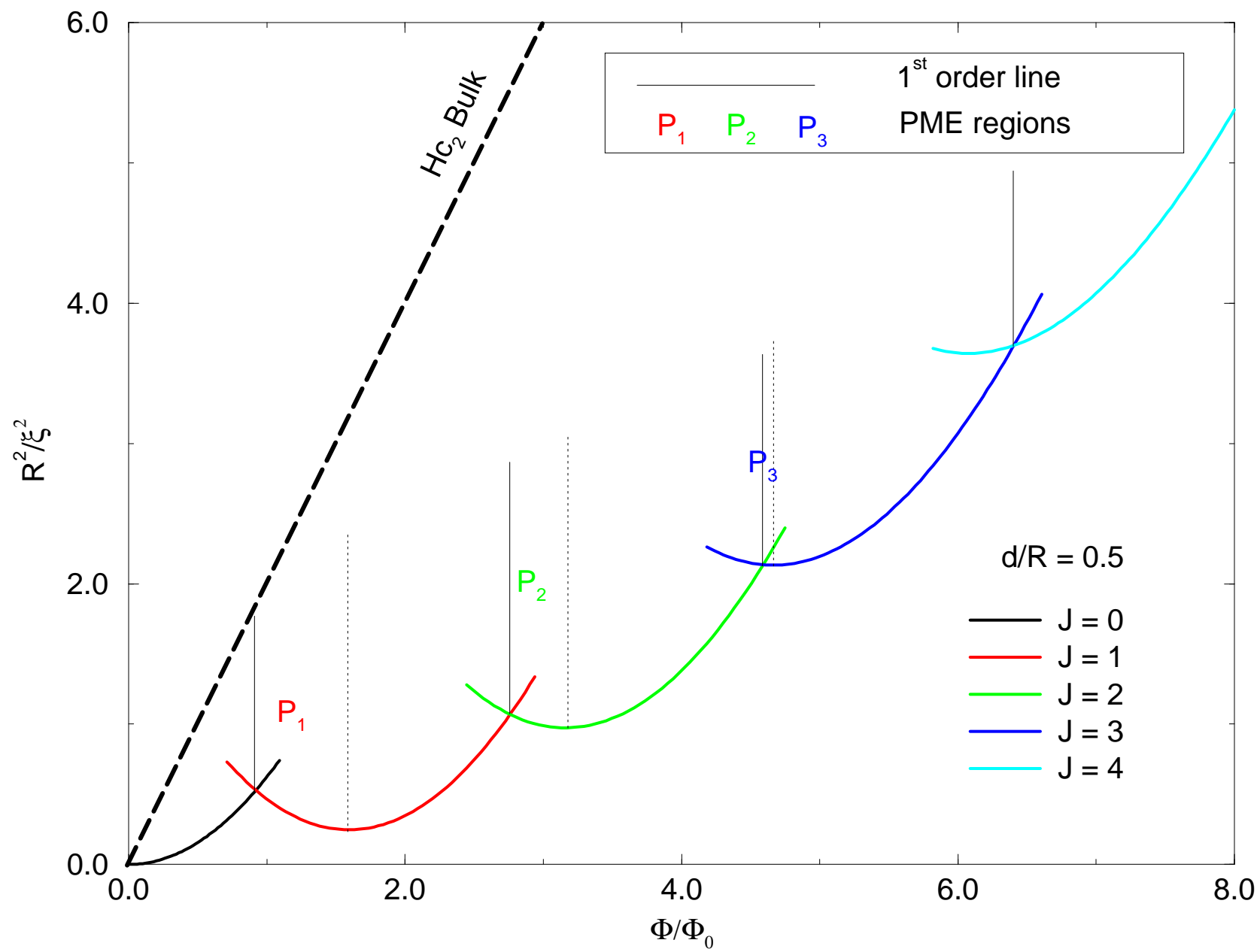


Fig 3

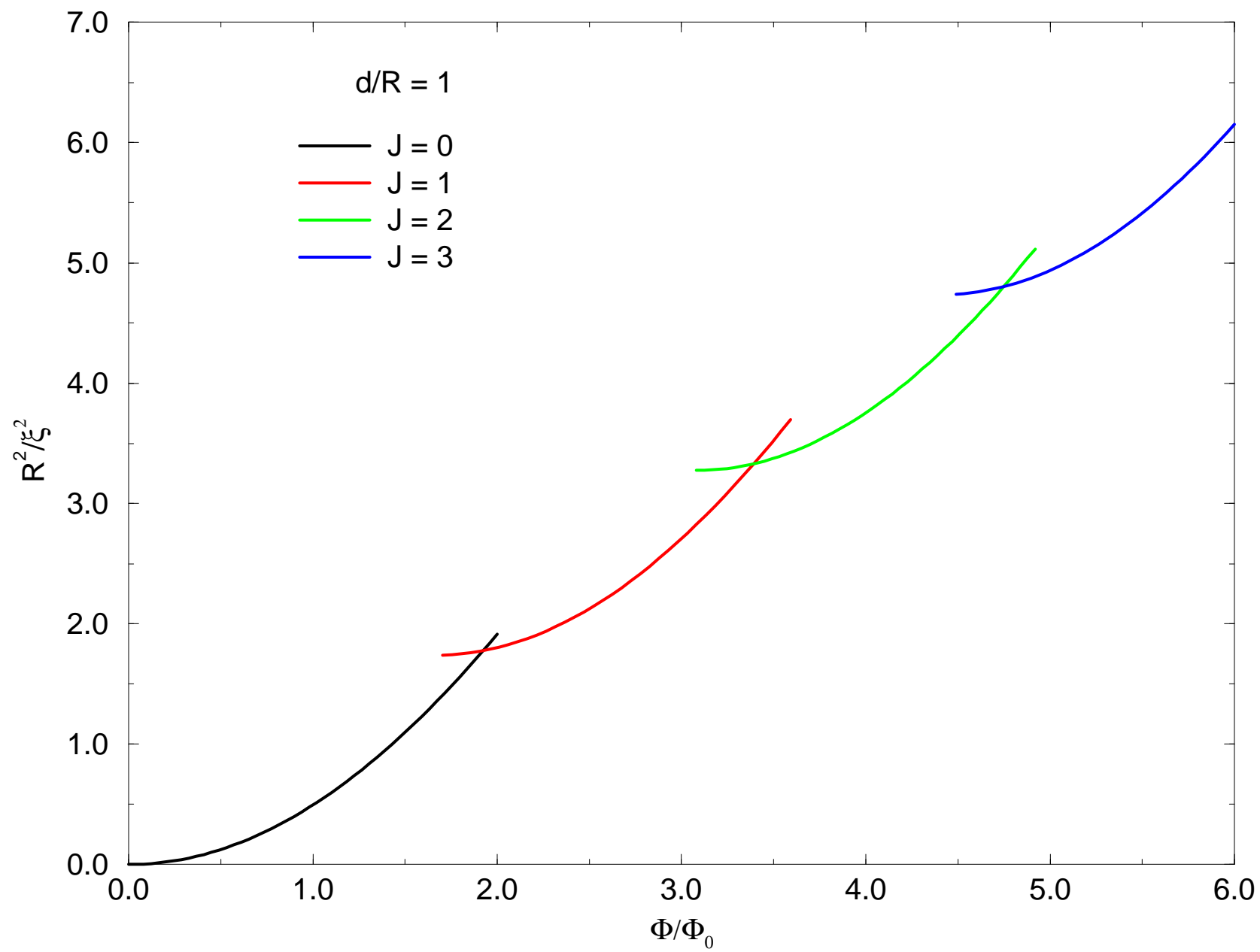


Fig 4

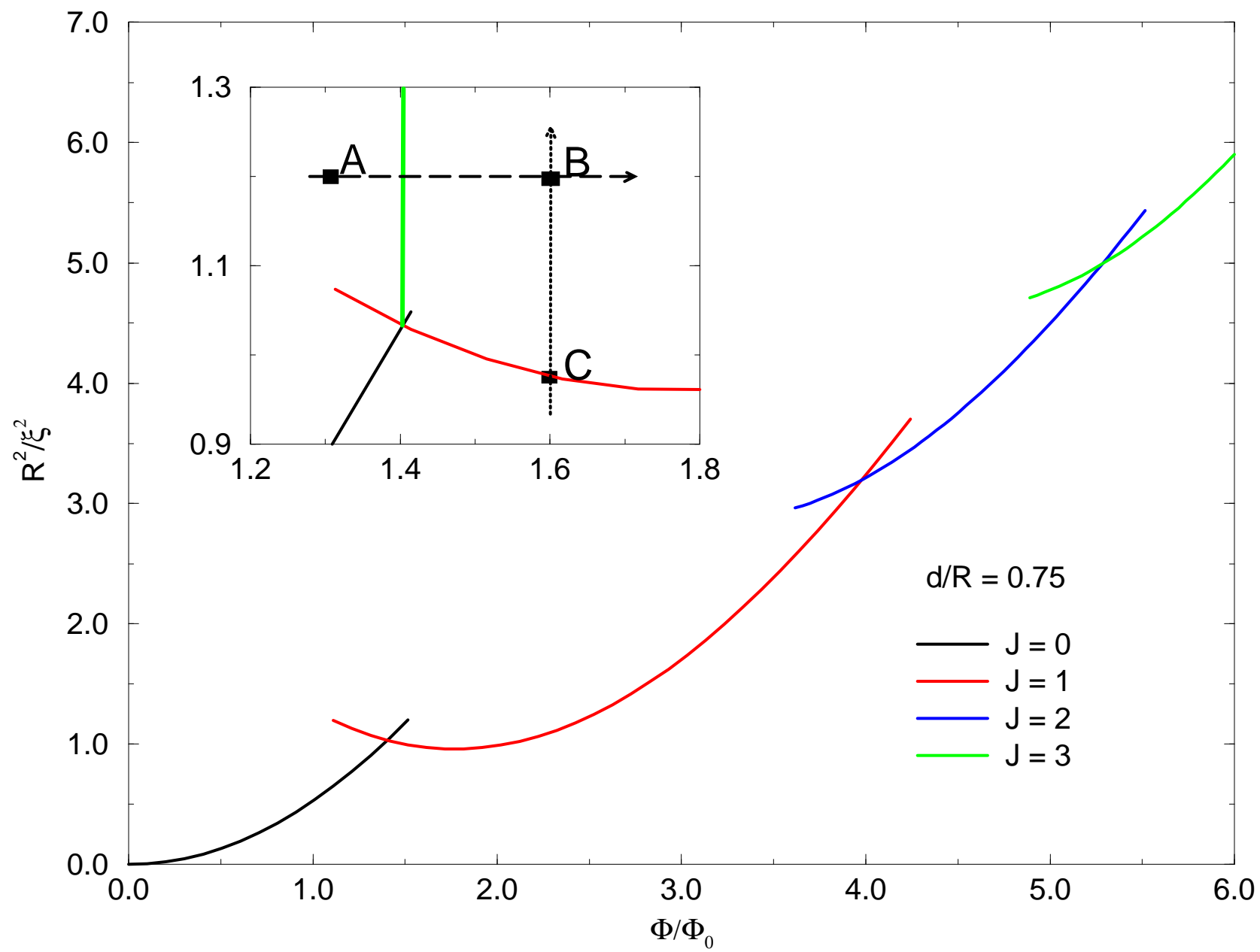


Fig 5a

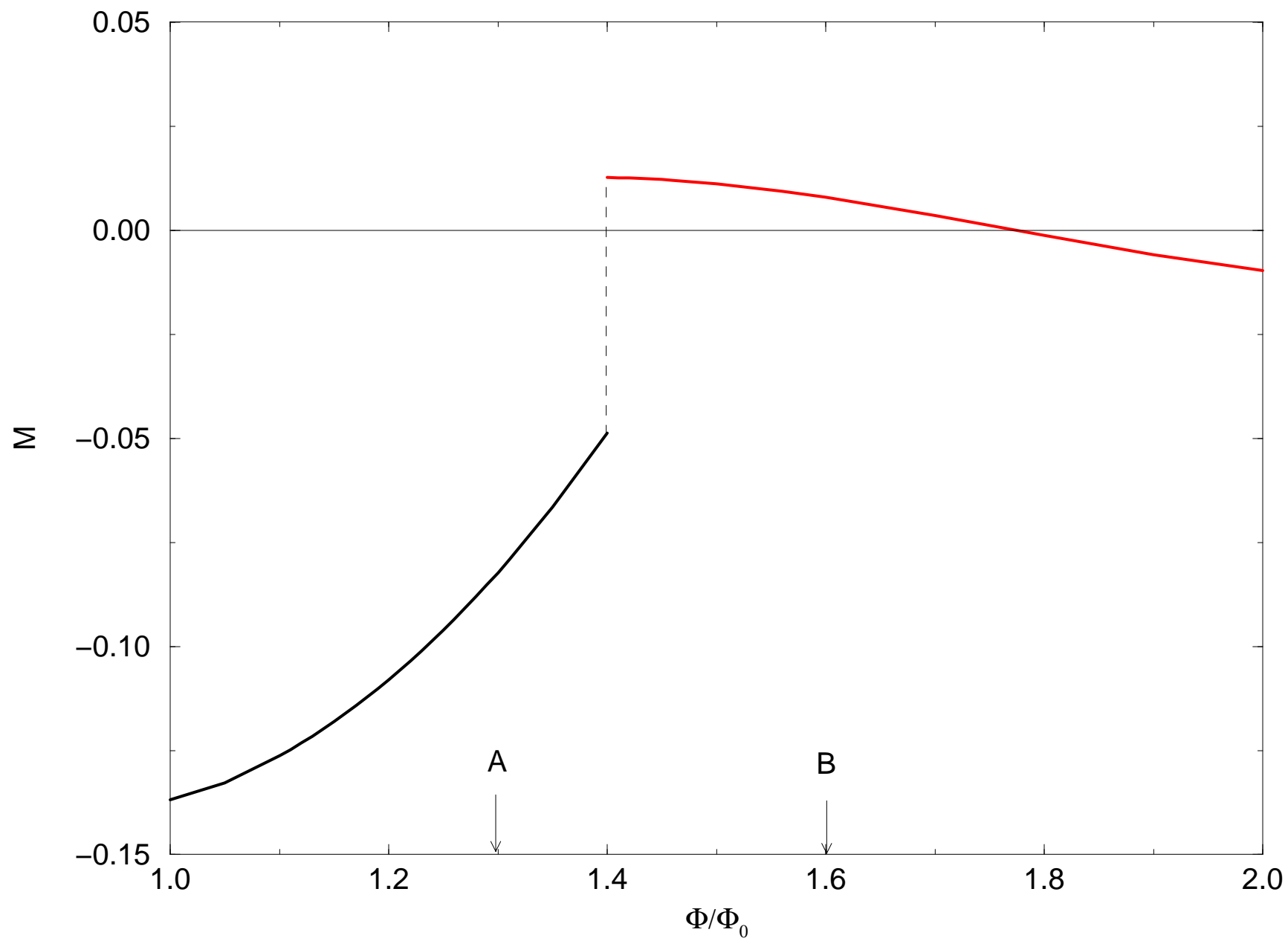


Fig 5b

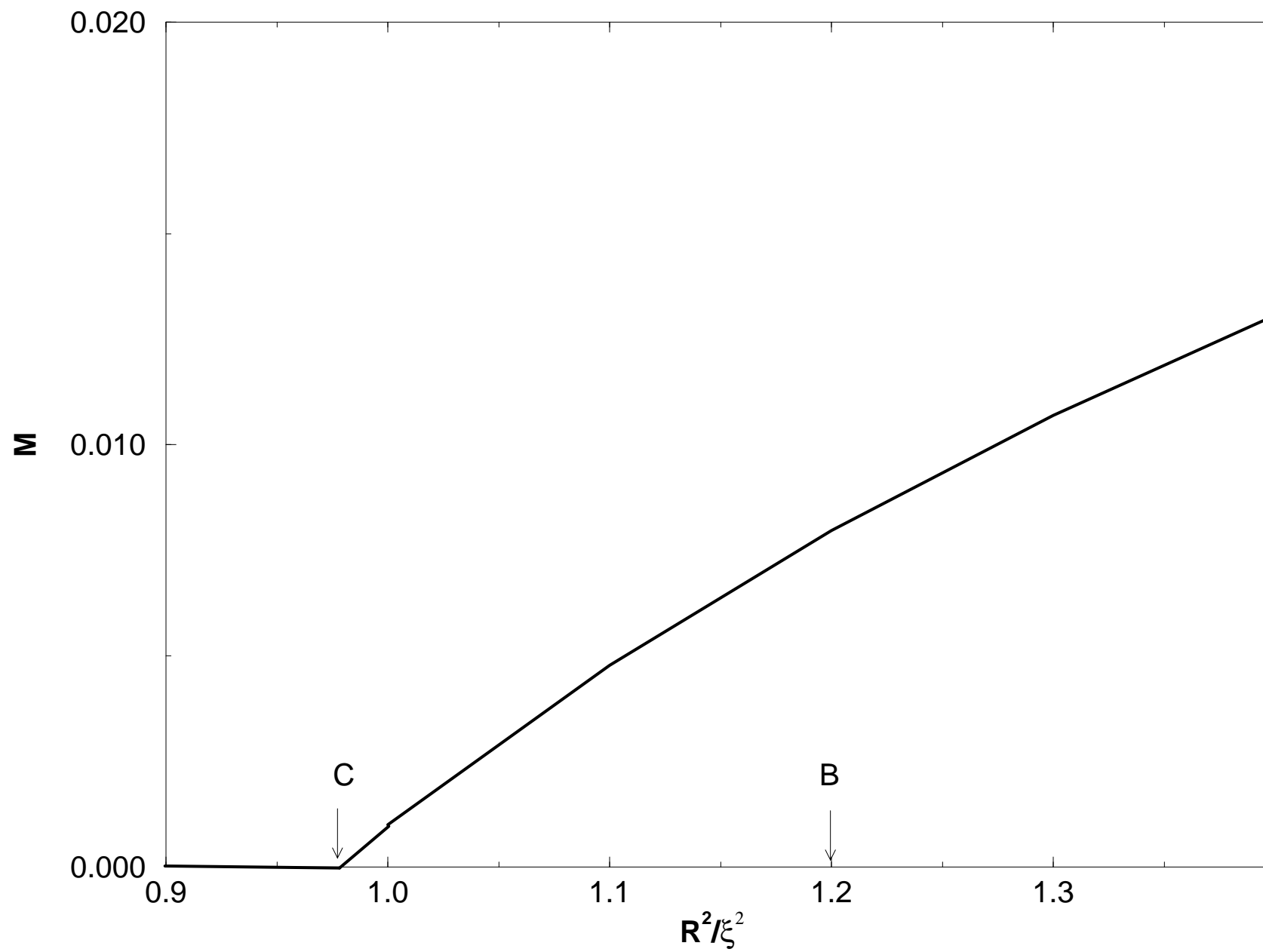


Fig 6

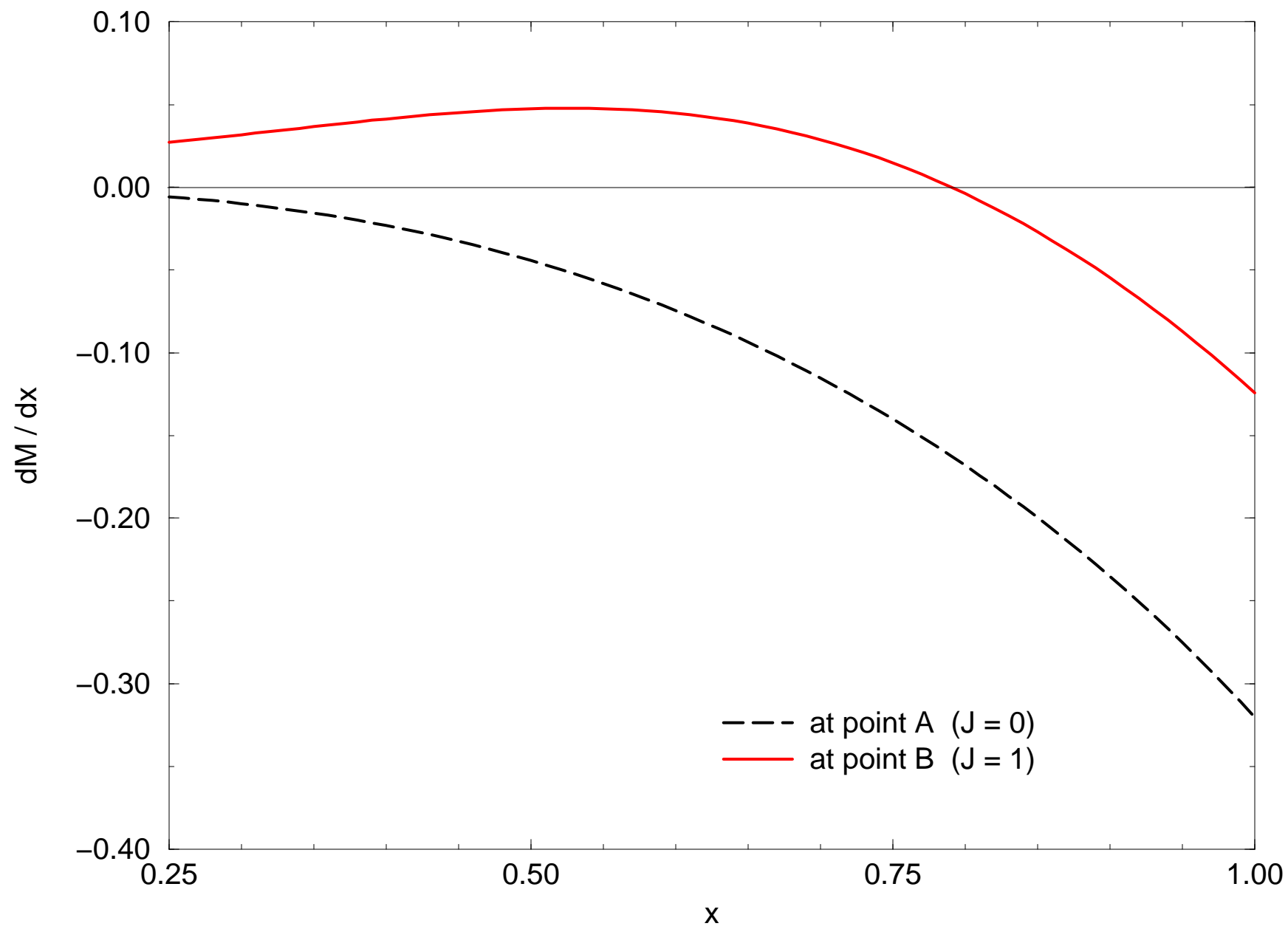


Fig 7

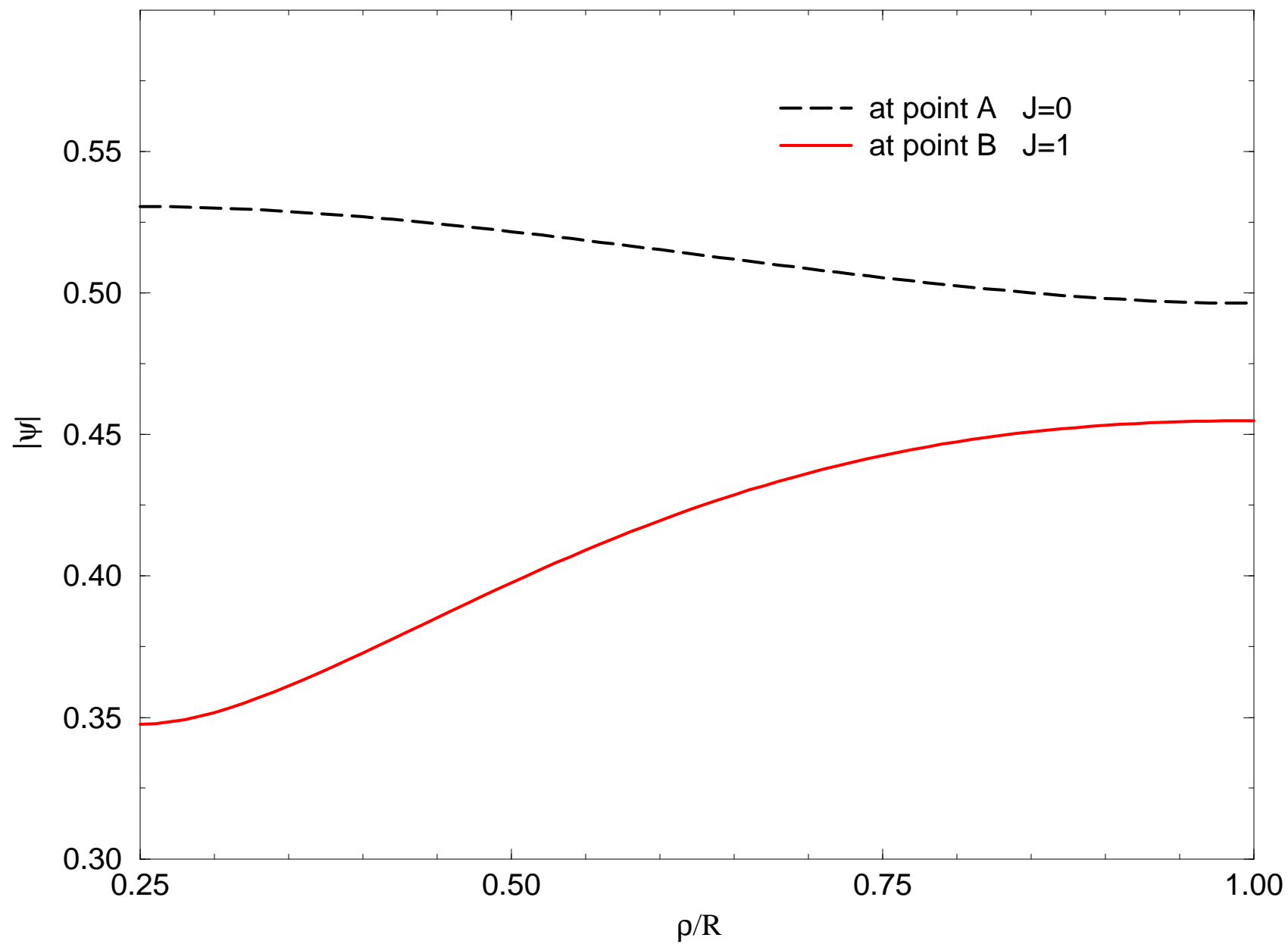


Fig 8

